

# Proton and Pion Production Relative to the Reaction Plane in Au + Au Collisions at AGS Energies

J. Barrette<sup>5</sup>, R. Bellwied<sup>9</sup>, S. Bennett<sup>9</sup>, R. Bersch<sup>7</sup>, P. Braun-Munzinger<sup>2</sup>, W. C. Chang<sup>7</sup>,  
W. E. Cleland<sup>6</sup>, M. Clemen<sup>6</sup>, J. Cole<sup>4</sup>, T. M. Cormier<sup>9</sup>, Y. Dai<sup>5</sup>, G. David<sup>1</sup>, J. Dee<sup>7</sup>,  
O. Dietzsch<sup>8</sup>, M. Drigert<sup>4</sup>, K. Filimonov<sup>5</sup>, S. C. Johnson<sup>7</sup>, J. R. Hall<sup>9</sup>, T. K. Hemmick<sup>7</sup>,  
N. Herrmann<sup>2</sup>, B. Hong<sup>2</sup>, Y. Kwon<sup>7</sup>, R. Lacasse<sup>5</sup>, Q. Li<sup>9</sup>, T. W. Ludlam<sup>1</sup>, S. K. Mark<sup>5</sup>,  
R. Matheus<sup>9</sup>, S. McCorkle<sup>1</sup>, J. T. Murgatroyd<sup>9</sup>, D. Miśkowiec<sup>2</sup>, E. O'Brien<sup>1</sup>, S. Panitkin<sup>7</sup>,  
T. Piazza<sup>7</sup>, M. Pollack<sup>7</sup>, C. Pruneau<sup>9</sup>, M. N. Rao<sup>7</sup>, E. Reber<sup>4</sup>, M. Rosati<sup>5</sup>, N. C. daSilva<sup>8</sup>,  
S. Sedykh<sup>7</sup>, U. Sonnadara<sup>6</sup>, J. Stachel<sup>3</sup>, E. M. Takagui<sup>8</sup>, S. Voloshin<sup>3\*</sup>,  
T. B. Vongpaseuth<sup>7</sup>, G. Wang<sup>5</sup>, J. P. Wessels<sup>3</sup>, C. L. Woody<sup>1</sup>, N. Xu<sup>7</sup>, Y. Zhang<sup>7</sup>, C. Zou<sup>7</sup>  
(E877 Collaboration)

<sup>1</sup> *Brookhaven National Laboratory, Upton, NY 11973*

<sup>2</sup> *Gesellschaft für Schwerionenforschung, 64291 Darmstadt, Germany*

<sup>3</sup> *Universität Heidelberg, 69120 Heidelberg, Germany*

<sup>4</sup> *Idaho National Engineering Laboratory, Idaho Falls, ID 83402*

<sup>5</sup> *McGill University, Montreal, Canada*

<sup>6</sup> *University of Pittsburgh, Pittsburgh, PA 15260*

<sup>7</sup> *SUNY, Stony Brook, NY 11794*

<sup>8</sup> *University of São Paulo, Brazil*

<sup>9</sup> *Wayne State University, Detroit, MI 48202*

(August 20, 2018)

Results are presented of an analysis of proton and charged pion azimuthal distributions measured with respect to the reaction plane in Au + Au collisions at a beam momentum of about 11A GeV/c. The azimuthal anisotropy is studied as a function of particle rapidity and transverse momentum for different centralities of the collisions. The triple differential (in rapidity, transverse momentum, and azimuthal angle) distributions are reconstructed. A comparison of the results with a previous analysis of charged particle and transverse

---

\*On leave from Moscow Engineering Physics Institute, Moscow, 115409, Russia

energy flow as well as with model predictions are presented.

## I. INTRODUCTION

Collective phenomena play an important role in heavy-ion collisions, but for a long time it was assumed that, at collision energies much greater than 1 GeV/nucleon, only longitudinal and azimuthally symmetric transverse radial flow would survive. During the last few years the situation has changed qualitatively. Anisotropic, directed as well as elliptic, flow has been observed at the BNL AGS [1,2], and strong indications of elliptic flow at the CERN SPS [3] have been demonstrated. The theoretical understanding of the effect and model calculations involving anisotropic flow have progressed significantly; different anisotropic flow patterns have been linked to such phenomena as quark-gluon plasma formation, softening of the equation of state [4–7], and mean-field effects during the fireball evolution [8–10]. The appropriate tools for flow studies at high energies have been developed [11,12]. It was also noticed that anisotropic flow could be important for other measurements, such as two-particle correlations [13,14]. Anisotropic flow has become an essential part of the global picture of heavy-ion collisions at ultrarelativistic energies [15]; it is considered one of the key tools to elucidate the dynamics of the collision.

In the current paper we present results of the analysis of anisotropic transverse collective flow of identified particles, protons and charged pions, detected in the E877 spectrometer in Au + Au collisions at a beam momentum of 10.8 and 11.4A GeV/c. The data were taken during the 1993 and 1994 AGS heavy-ion runs. Using calorimeter data we reconstruct the reaction plane event-by-event, and analyze the particle production with respect to this reaction plane. A similar analysis of charged particle multiplicity and transverse energy flow presented in [2] displayed a strong directed flow as well as an elliptic flow with the primary axis in the reaction plane, *i.e.* perpendicular to the direction of the “squeeze-out” effect observed at lower energies [16]. Here, using the E877 spectrometer data, we apply the same procedure to determine the triple differential distributions  $d^3N/(dy p_t dp_t d\phi)$  of identified protons and charged pions.

The paper is organized as follows. After a description of the apparatus we discuss the procedure of the analysis. In the subsequent sections we present first the results of the Fourier analysis of azimuthal particle distributions in different rapidity bins and for different centralities of the collision. These results are, to a large extent, independent of the uncertainties in the spectrometer efficiency and the detector acceptance. Then the results on azimuthal anisotropies and related quantities (such as the mean transverse momentum projected into the reaction plane  $\langle p_x \rangle$ ) are discussed. Different flow scenarios are discussed from the point of view of the observed dependence of the flow signal on the transverse momentum  $p_t$  of the particle. We compare our measurements with the evaluation of nucleon and pion flow derived from the measurements of charged particle and transverse energy flow [2], as well as with model predictions (RQMD versions 1.08 and 2.3 [10,17]).

## II. APPARATUS

The E877 apparatus is shown in Fig. 1. In the E877 setup, charged particles, emitted in the forward direction and traversing the collimator ( $-134 < \theta_{horizontal} < 16$  mrad,  $-11 < \theta_{vertical} < 11$  mrad), are analyzed by a high resolution magnetic spectrometer. The spectrometer identifies particles via simultaneous measurements of momentum and velocity. The momentum of each particle is measured using two drift chambers (DC2 and DC3, position resolution about  $300 \mu\text{m}$ ) whose pattern recognition is aided by four multi-wire proportional chambers (MWPC). The average momentum resolution is  $\Delta p/p \approx 3\%$  limited by multiple scattering. A time-of-flight hodoscope (TOFU) located behind the tracking chambers provides the time-of-flight with a typical resolution of 85 ps. The spectrometer acceptance covers mostly the forward rapidity region with transverse momentum coverage including  $p_t = 0$ . Further discussion of the acceptance for different particle species can be found in [18].

A clean particle identification is particularly crucial for the study of flow since the extracted signal may be different for different particle species both in magnitude and in sign. A small admixture in the particle sample of other particle species could therefore heavily bias the final results. Consequently, in the current analysis, strict requirements are applied for particle identification. Using the measured momentum and velocity of the particle we

calculate the particle mass. In a plot of momentum *vs.* the square of the particle mass  $m^2$  we select entries in the region of  $\pm 1.5 \sigma_{m^2}(p)$  around the  $m^2$  peak of the particle under study and reject all entries within a  $3 \sigma_{m^2}(p)$  region of another particle species. Here,  $\sigma_{m^2}(p)$  represents the standard deviation of the (Gaussian) mass-squared distribution at a given particle momentum  $p$ .

The determination of the centrality of the collision and of the reaction plane orientation are made using the transverse energy flow measured in the target calorimeter (TCal), and participant calorimeter (PCal). Both calorimeters have  $2\pi$  azimuthal coverage and, combined together, they provide nearly complete polar angle coverage as viewed from the nucleus-nucleus center of mass system: TCal and PCal cover the pseudorapidity regions  $-0.5 < \eta < 0.8$  and  $0.8 < \eta < 4.2$ , respectively [2,19]. The pseudo-rapidity  $\eta = -\ln \tan(\theta/2)$  is defined in terms of the polar angle  $\theta$  in the laboratory frame.

### III. ANALYSIS

The structure of the analysis is very similar to that used in [2], and many details can be found there. Here, the distributions  $d^3N/(p_t dp_t dy d\phi)$  of identified protons and charged pions are generated in a coordinate system where the  $x$ - and  $z$ -axes span the reaction plane. The azimuthal angle in this system is defined as  $\phi = \phi_{lab} - \Psi_1$ , where  $\Psi_1$  is the reaction plane angle, measured for every event using the direction of the transverse energy flow in TCal and PCal, and  $\phi_{lab}$  is the azimuthal angle of an individual particle in the laboratory frame. The  $x$ -axis is defined in such a way that it points in the direction of the transverse energy flow at forward rapidities. The transverse momentum components  $p_x$  and  $p_y$  of identified particles are evaluated in this coordinate system, and the particle distributions with respect to the reaction plane are constructed. The azimuthal anisotropy of particle production is studied by means of Fourier analysis of azimuthal distributions [1,2,12]. This yields the rapidity, transverse momentum, and centrality dependence of the Fourier coefficients  $v_n$  (amplitude of  $n$ -th harmonic) in the decomposition:

$$E \frac{d^3N}{d^3p} = \frac{d^3N}{p_t dp_t dy d\phi} = \frac{1}{2\pi} \frac{d^2N}{p_t dp_t dy} (1 + 2v'_1 \cos(\phi) + 2v'_2 \cos(2\phi) + 2v'_3 \cos(3\phi) + \dots). \quad (1)$$

The E877 spectrometer provides full  $2\pi$  acceptance in the spectrometer only for a very limited  $p_t$  range (approximately  $p_t \leq 50$  MeV/c), but the triple differential multiplicity is constructed in full, using the  $2\pi$  range of the reaction plane angle distribution. Note that the coverage of the calorimeters used for the reaction plane determination does not overlap with the spectrometer coverage, and thus the analysis is largely free from problems related to auto-correlations.

Similarly to the analysis presented in [2], the reaction plane angle  $\Psi_1$  is determined in four non-overlapping pseudorapidity windows. The 'reaction plane resolution', i.e. the accuracy with which the reaction plane orientation is determined, is evaluated by studying the correlation between flow angles determined in different windows. Finally, the flow signals are corrected for this resolution. Details of this procedure are described in [2]. In short, the true value of each Fourier coefficient  $v_n$  is obtained by:

$$v_n = v'_n / \langle \cos(n(\Psi_1 - \Psi_R)) \rangle, \quad (2)$$

where  $v'_n$  is the observed signal, and  $\langle \cos(n(\Psi_1 - \Psi_R)) \rangle$  is the mean cosine of the difference of the reconstructed ( $\Psi_1$ ) and true ( $\Psi_R$ ) reaction plane angles, characterizing the reaction plane resolution. The values of  $\langle \cos(n(\Psi_1 - \Psi_R)) \rangle$  are evaluated as outlined in [2]. As a result we obtain the true azimuthal distribution with respect to the reaction plane orientation:

$$E \frac{d^3 N}{d^3 p} = \frac{1}{2\pi} \frac{d^2 N}{p_t dp_t dy} (1 + 2v_1 \cos(\phi_{lab} - \Psi_R) + 2v_2 \cos(2(\phi_{lab} - \Psi_R)) + \dots). \quad (3)$$

The E877 spectrometer has a relatively small azimuthal coverage. Due to this, the analysis of azimuthal anisotropies is rather sensitive to biases of different kinds, which could simulate an event anisotropy and propagate to the final results. For instance, during the off-line analysis, it was found that a small fraction of the recorded events ( $\leq 2-4\%$ ) have an anomalously high number of hits in the drift chambers. In these events the hit density was too high to perform reliable tracking and the high occupancy of the spectrometer was found to be correlated with the orientation of the reaction plane. A bias due to this was avoided by removing these events from the analysis completely and not only from the sample used to generate spectra. The tracking efficiency in the spectrometer (typically on the order of 90%) depends slightly on the spectrometer occupancy. A special correction for this effect was developed and checked by a Monte-Carlo simulation. The correction is based on the

weighting of each track in accordance with the local track densities in the drift chambers and time-of-flight wall. Due to different gain factors and dead towers in the calorimeters the distribution in the reconstructed reaction plane angle is generally not flat. Special precaution was taken to make the reaction plane angle distribution as flat as possible and to remove possible biases (see Appendix A).

The Fourier coefficients of azimuthal distributions evaluated by the procedure described above (and corrected for the reaction plane resolution), are combined with the measurements of  $p_t$  and rapidity spectra [18]. In this way the triple differential distributions in  $y$ ,  $p_t$ , and  $\phi$  (see Equation (3)) are determined and analyzed.

## IV. RESULTS

### Directed Flow

Anisotropic flow reveals itself already in the dependence on the azimuthal emission angle of the inverse slope parameter of the invariant spectra  $E d^3 N / d^3 p = d^3 N / (p_t dp_t dy d\phi) = d^3 N / (m_t dm_t dy d\phi)$  when plotted as a function of  $m_t - m$  for a given  $\phi$ . Here,  $m_t = \sqrt{p_t^2 + m^2}$  is the transverse mass. We extract the inverse slope parameter  $T_B(\phi)$  by fitting the spectra in the region  $m_t - m > 0.1$  GeV/ $c^2$  by a thermal (Boltzmann) function

$$E \frac{d^3 N}{d^3 p} \propto m_t \exp \left( -\frac{m_t - m}{T_B(\phi)} \right). \quad (4)$$

The shape of the spectra is not perfectly reproduced by this function, and in order to obtain a good quality description of the spectra in the entire  $m_t$  region, the weights of all points were chosen to be equal for the fit and not in accordance with statistical errors.

In Fig. 2 we show the  $m_t$  spectra of protons emitted into the rapidity interval  $2.8 < y < 2.9$  at different angles relative to the reaction plane together with these thermal fits for different centralities. Clearly, the spectra of protons emitted in the direction of flow ( $\phi=0$ ) are significantly flatter than those of protons emitted in the opposite direction ( $\phi = \pi$ ). To visualize the angular dependence of the inverse slope parameters the results from the fit are shown in Fig. 3 for three rapidity intervals. Here  $T_B$  is plotted as a function of the azimuthal emission angle. The results are presented for four centrality regions, selected in accordance

with PCal  $E_T$  and corresponding to the values of  $\sigma_{top}(E_T)/\sigma_{geo} \approx 23\text{--}13\%$ ,  $13\text{--}9\%$ ,  $9\text{--}4\%$ , and  $<4\%$  (see Fig. 4 in [2]). The value of  $\sigma_{top}(E_T)$  is obtained by an integration of  $d\sigma/dE_T$  from a given value of  $E_T$  to the maximal one observed, and the geometric cross section is defined as  $\sigma_{geo} = \pi r_0^2 (A^{1/3} + A^{1/3})^2 = 6.13$  b, with  $A = 197$  and  $r_0 = 1.2$  fm.

The results shown in Figs. 2 and 3 are not corrected for the reaction plane resolution. The correction would increase the difference between the maximal and minimal values of  $T_B$  by about a factor of 1.5. Such a correction (in terms of  $T_B$ ) is rather complicated; for the quantitative description of the flow effects we use a Fourier analysis of the azimuthal distributions [1,2,12] where all corrections are implemented.

We quantify directed flow by  $v_1$ , the amplitude of the first harmonic in the Fourier decomposition of the azimuthal particle distribution defined in Equation (1) and corrected for the reaction plane resolution. The coefficient  $v_1$  is analyzed as a function of transverse momentum for different rapidity bins and collision centralities. The results for  $v_1(p_t)$ , corrected for the reaction plane resolution, are presented in Figs. 4–6 for protons and charged pions.

The error-bars shown in all figures represent statistical errors only. The systematic uncertainties have mostly two sources: i) The uncertainty in the determination of the reaction plane resolution leading to a relative error in  $v_1$  of the order of 5–10%, similar for all particle species. ii) The uncertainty in the occupancy correction, the accuracy of which we estimate, by inspection of Monte-Carlo simulations, to be of the order of 20–30%. The correction itself is different for different particle species. It is negligible for positive pions (and for negative pions from the 1993 run), which are registered in the low occupancy region of the spectrometer. The correction is maximal, and reaches absolute values of about 0.1 for the data shown, for protons at low  $p_t$  and/or high rapidities. The rapidly increasing uncertainty in the occupancy correction in the spectrometer region close to the beam limits our measurements of proton flow at very low  $p_t$ . Multiplying the uncertainty in the occupancy correction with its absolute value we end up with a systematic error in the absolute value of  $v_1$  of about 0.03 where the correction is maximal.

As can be seen from Fig. 4, proton emission is very strongly correlated with the orientation of the reaction plane. Protons of larger  $p_t$  have larger values of  $v_1$  with some tendency to saturation in the highest  $p_t$  region. The largest flow signal observed corresponds to a dif-

ference in the high  $p_t$  proton yields along ( $\phi = 0$ ) and opposite to the flow direction ( $\phi = \pi$ ) of almost a factor of 10 (as can also be seen in Fig. 2). Both positive (Fig. 5) and negative (Fig. 6) pions exhibit weak flow in the direction opposite to that of protons (negative values of  $v_1$ ) over most of the  $p_t$  region studied. The maximum negative values of  $v_1^\pi$  are about  $-0.1$ , significantly less in magnitude than the flow signal observed for protons.<sup>1</sup>

Independent of any flow scenario  $v_1(p_t)$  must vanish at  $p_t = 0$ , due to the continuity of the spectra. The small non-zero values of  $v_1$  for the lowest  $p_t$  bin in Figs. 5 and 6 (for low centralities and rapidities close to beam rapidity; positive for negative pions and negative for positive pions) are mostly due to the finite bin size of the data. The details of the behavior of  $v_1$  at very low  $p_t$  are presented in Fig. 7 where we show, in the same plot, the results for positive and negative pions in the rapidity region  $3.2 < y < 3.6$  for two different centralities and with much finer binning.

Not only are the sign and magnitude of the flow signal very different for protons and pions but also the functional dependence on  $p_t$  varies with particle species. The  $v_1$  values for protons grow almost linearly with  $p_t$  over the entire  $p_t$  region. Inspecting the transverse momentum dependence of  $v_1$  for pions one can distinguish three regions in  $p_t$ : i) The very low  $p_t$  region (below  $p_t \approx 0.1$  GeV/c) where in fact the flow signals of positive and negative pions are different. Positive pions show  $v_1$  values decreasing rapidly and monotonously towards negative values. Conversely, for negative pions, the flow signal becomes at first positive, reaches a peak at about  $p_t=0.01-0.02$  GeV/c, and then decreases towards negative values where the flow signals for both pion charges merge. This is best seen in Fig. 7. The merging point appears to depend on centrality, moving to lower  $p_t$  for the more central events. ii) An intermediate region, approximately at  $0.1 < p_t < 0.3$  GeV/c, where  $v_1$  is negative and only weakly dependent on  $p_t$  for both pion charges. And finally iii) the high  $p_t$  region where  $v_1$  begins to rise and becomes positive. There is in fact a very systematic rapidity dependence of the zero-crossing point: It moves to lower  $p_t$  values with increasing rapidity occurring at

---

<sup>1</sup>Due to a “hole” in the  $p_t$  acceptance of negative pions for the magnetic field polarity used during the 1994 run we have combined data from the 1994 run and from the lower statistics 1993 run (shown in Fig. 6 as open points), where data exist for both polarities of the magnetic field.

$p_t = 0.5-0.6$ ,  $0.4-0.5$ , and  $0.3-0.4$  GeV/c for the three rapidity bins at  $y=2.8-3.2$ ,  $3.2-3.6$ , and  $3.6-4.0$ , respectively.

The centrality dependence of all flow signals is rather pronounced; in the analyzed centrality region the magnitude of flow for all particles decreases for more central collisions. Directed flow of beam rapidity protons shows a relatively smaller centrality dependence than that of protons at lower rapidities (see also Fig. 9 below).

### Higher Harmonics in Azimuthal Distributions

Higher order harmonics ( $v_2$  and  $v_3$ ) in the particle azimuthal distributions have also been analyzed. The accuracy in the evaluation of the contribution of higher harmonics deteriorates with increasing order due to the finite reaction plane resolution (see the discussion in [2]). This results in larger relative errors. Our results for the proton elliptic flow (amplitude of the second harmonic in the proton azimuthal distributions) as a function of transverse momentum are presented in Fig. 8. A clear positive signal is observed in the high  $p_t$  region for rapidities of 2.6 and larger. There is an indication that the signal moves to higher  $p_t$  values with decreasing rapidity. This combined with the smaller acceptance in  $p_t$  at rapidities below 2.6 may be the reason that no significant signal is observed there. In our previous measurements of transverse energy and charged particle flow [2] a clear signal of elliptic flow was observed at all values of pseudorapidity. The observed positive values of  $v_2$  correspond to an elliptically shaped distribution with the major axis lying in the reaction plane. This orientation of the elliptic component is perpendicular to what was measured at lower beam energies [16].

Within our spectrometer acceptance, pions do not exhibit elliptic flow at the level of 2–3%.

The (absolute) accuracy in measuring  $v_3$  is about 0.1. For all particles, rapidities, and centralities of the collision the observed signals are consistent with zero within this accuracy.

## Mean Directed Transverse Momentum

Weighted with  $p_t$  and its probability distribution the coefficient  $v_1$  yields  $\langle p_x \rangle$ , the mean value of the transverse momentum projected onto the reaction plane:

$$\langle p_x \rangle = \frac{1}{N} \int v_1(p_t) p_t \frac{dN}{dp_t} dp_t. \quad (5)$$

Like any other integral quantity,  $\langle p_x \rangle$  contains less information than  $v_1$ . We nevertheless calculate this quantity in order to compare our results with results from other experiments and model predictions. This is done by using spectra [18] measured with the same apparatus. Our results of the value of  $\langle p_x \rangle$  for protons at different centralities are shown in Fig. 9. Due to the experimental acceptance in  $p_t$ , a model-independent evaluation of this quantity is possible only at rapidities  $y > 2.8$ . Where it becomes necessary, we extrapolate  $dN/dp_t$  to high  $p_t$  using a thermal parameterization (as used e.g. in Equation (4)). The filled points in Fig. 9 correspond to  $\langle p_x \rangle$  calculated in accordance with Equation (5), using the parameterization of  $v_1(p_t)$  shown in Fig. 4 as the solid (upper) curves to extrapolate  $v_1$  into the  $p_t$  range not measured (for an analytic expression of this parameterization see Equation (11) below). The small difference between the parameterization and the data in the low  $p_t$  region does not contribute visibly to the final result for  $\langle p_x \rangle$ . The contribution of the non-measured high  $p_t$  part of the spectra to  $\langle p_x \rangle$  is relatively small at rapidities  $y \geq 2.8$  (less than 10%), where the acceptance in  $p_t$  is large. At rapidity  $y = 2.5$  this contribution accounts for about 40% of the value of  $\langle p_x \rangle$ . The error-bars shown do not include the uncertainty in the effective slope parameters used for the extrapolation of the  $p_t$  spectra or any systematic uncertainty associated with the extrapolation of  $v_1$ .

In order to assess the systematic error we evaluate the same quantity ( $\langle p_x \rangle$ ) by using a different parameterization of the invariant triple differential distribution with  $\langle p_x \rangle$  as a parameter. We use the following functional form to parameterize  $d^3N/d^3p$  of protons in a given rapidity bin:

$$d^3N/d^3p \propto m'_t \exp\left(-\frac{m'_t - m}{T}\right), \quad (6)$$

$$m'_t = \sqrt{(p_x - \langle p_x \rangle)^2 + p_y^2 + m^2}, \quad (7)$$

*i.e.* a thermal distribution with respect to an origin displaced along the  $p_x$ -axis. With the

effective slope parameters taken from [18] we use function (6) to fit the experimental values of  $v_1(p_t)$  (see Fig. 4, dashed (lower) curves). The extracted values of  $\langle p_x \rangle$  are shown in Fig. 9 as open symbols. The difference between the results obtained with the two different parameterizations (filled and open symbols in Fig. 9) gives an idea of the systematic uncertainty of the results, not including the systematic uncertainty in  $v_1$  itself in the range where it is measured (see above). The latter could be important for the lowest rapidity region of  $2.2 < y < 2.4$ , where the flow signal is very small; there we estimate an associated systematic uncertainty of  $\langle p_x \rangle$  of about 20 MeV.

The evaluation of  $\langle p_x \rangle$  values for pions was done by convoluting the experimental values of  $v_1(p_t)$  with the spectra without any extrapolation to the high  $p_t$  region. This is possible due to the relatively large  $p_t$  acceptance for pions in the rapidity interval studied. The extracted values of  $\langle p_x \rangle$  for pions are about an order of magnitude smaller than those for protons. The results for the centrality region  $\sigma_{top}/\sigma_{geo} \approx 9\text{--}13\%$  (centrality 2) are presented in Fig. 11 (squares and triangles) together with the corresponding proton results and will be discussed below.

## V. DIRECTED FLOW DISCUSSION

### Moving thermalized source *vs.* absorption

One of the simplest pictures of directed flow would be the motion in the transverse plane of a thermalized source, localized in rapidity. Assuming for the simplest case of no radial expansion, the invariant momentum spectrum for particle emission from a thermalized source is described by:

$$\frac{1}{m_t} \frac{dN}{dm_t dy d\phi} \propto E^* e^{-E^*/T}, \quad (8)$$

where  $T$  is the temperature, and  $E^*$  is the particle's energy in the rest frame of the source. In the case of a thermal source moving in  $x$ -direction with velocity  $\beta_x$  (which we call the directed flow velocity), the value of  $E^*$  can be obtained by a Lorentz transformation:

$$E^* = \gamma \tilde{E} - \beta_x \gamma_x p_t \cos(\phi), \quad (9)$$

where  $\gamma_x = 1/\sqrt{1 - \beta_x^2}$ , and the energy  $\tilde{E}$  is evaluated in the system moving longitudinally with the same velocity as the source,  $\tilde{E} = m_t \cosh(y - y^*)$ . Here  $y^*$  is the source rapidity. Using Equations (8) and (9) one can evaluate the first Fourier coefficient  $v_1$  by direct integration to yield

$$v_1 = \frac{I_1(\xi) - (\xi I_0(\xi) - I_1(\xi))T/\tilde{E}}{I_0(\xi) - \xi I_1(\xi)T/\tilde{E}}, \quad (10)$$

where  $\xi = p_t \beta_x \gamma_x / T$ , and  $I_0(\xi)$ ,  $I_1(\xi)$  are the modified Bessel functions. For protons,  $m_t \gg T$  and  $v_1$  does not depend on the, generally unknown, value of  $y^*$ . Since we expect that  $\beta_x \ll 1$  it is useful to note that in that case, for relatively small values of  $p_t$ ,  $v_1$  depends almost linearly on  $p_t$ :

$$v_1 \approx \frac{I_1(\xi)}{I_0(\xi)} \quad \left( \approx \frac{p_t \beta_x}{2T} \right). \quad (11)$$

The solid lines shown in Fig. 4 correspond to fits to the data using Equation (11) and inverse slope parameters  $T_B$  from [18] as  $T$ . Overall, the fit is rather good. Taking into account that, in general, one cannot interpret the inverse slope parameters  $T_B$  as a source temperature we would like to note that Equations (10,11) are still valid for the case that the invariant spectra at a fixed rapidity have a thermal shape with some effective temperature constant.

In Fig. 10, the extracted values of  $\beta_x$  of the proton source are shown for different collision centralities as a function of proton rapidity. One can see that the transverse source velocity grows with increasing rapidity, possibly peaking around rapidity  $y=3.1$ . The maximum values are about 10 % of the speed of light. This transverse velocity is found to decrease with increasing centrality of the collision. These results have to be put into perspective with the transverse expansion velocities fitted to spectra of various particle species in the same reaction and close to mid-rapidity: in such an analysis transverse expansion velocities of about 50 % of the speed of light are required to describe the data [15]. This effect is largest in central collisions. The transverse expansion velocity decreases away from mid-rapidity.

Looking more closely at the fits in Fig. 4 one notices a small deviation of the fit using Equation (11) from the data at small transverse momenta ( $p_t < 0.1$  GeV/c) and at rapidities  $y \leq 2.8$ . There, protons exhibit a weaker or even opposite flow than expected from the simple model discussed above. This could be an indication of transverse expansion as pointed out in reference [20]. There, it is shown that, depending on the relative magnitude of the sideward

flow velocity  $\beta_x$  and the transverse expansion velocity  $\beta_t$ , a reduction or even sign change of  $v_1$  at small  $p_t$  is possible.

For pions we observe a dependence of  $v_1$  on  $p_t$  very different from that for protons. It implies that the physics of pion flow is different from that of a moving source alone (just as one would expect). A possible explanation of the pion flow signal could be found in a superposition of different effects: Absorption in nuclear matter, Coulomb interaction with comoving protons, and sideward motion of the source.

For pions produced in the center of the collision volume and moving in forward direction with velocities close to speed of light, one would expect more nuclear matter on the side characterized by the direction of nucleon flow (positive  $x$  in our notation) and, consequently, more absorption. The effect of pion absorption on nucleons with energy-, or for a fixed rapidity,  $p_t$ -independent cross section would lead to a negative and constant value of  $v_1(p_t)$ . Such absorption should be comparable for positive and negative pions. On the other hand, it is known that in the relevant momentum range the pion-nucleon elastic and total cross sections are strongly peaked at the  $\Delta$  resonance [21]. In a frame where the nucleon is at rest the cross section peaks at a pion momentum of 0.3 GeV/c and falls off rapidly for larger momenta. If the absorption of pions would occur on nucleons of the same rapidity, this would mean that the negative values of  $v_1$  should increase towards zero for  $p_t \geq 0.3$  GeV/c. Most of the pions we observe are in a rapidity range where there are very few nucleons (forward of beam rapidity). Indeed, analysis of the proton rapidity distribution indicates [15] that nucleon sources (fireballs) are distributed evenly over plus and minus one unit of rapidity in the c.m. frame, *i.e.* that the most forward nucleon source is at rapidity 2.5 in the laboratory. For pions at rapidities 3.0, 3.4, and 3.8 this would imply that absorption effects should decrease for transverse momenta larger than 0.30, 0.27, and 0.20 GeV/c. The data indeed show this trend with rapidity at about the  $p_t$  values expected (see Figs. 5,6, and 7).

At the same time Coulomb interaction with positively charged nuclear matter would be different for pions of different charge, and could qualitatively explain the difference in flow signals at very low  $p_t$  shown in Fig. 7. Negative pions are attracted to the protons leading to positive values of  $v_1$  (as argued in the case of absorption on nucleons above) while positive

pions are repelled leading to more negative values of  $v_1$ .

The rise of  $v_1$  for pions towards large  $p_t$  could reflect the sideward motion of the source, the same way it does for protons.

### Comparison with the results on $N_c$ and $E_T$ flow

Fig. 11 shows, for the  $E_T$ -range 200-230 GeV, the mean directed transverse momenta for protons, positive, and negative pions. Due to the acceptance of the spectrometer the proton and pion results are forward of rapidity 2.2 and 2.8, respectively. Results were obtained using Equation (11) to complete the integral (5) beyond the range where  $v_1$  is measured. The error-bars shown include an error in the effective temperature of about 7 % in addition to the statistical errors. The symmetry of the collision system allows reflection of these results about mid-rapidity, shown in Fig. 11 by the open symbols, providing values for protons backward of rapidity 0.9 and for pions backward of rapidity 0.3. To fill the gap at intermediate rapidities we use our measurement of the flow signal in transverse energy  $E_T$  and charged particle multiplicity  $N_c$  as published in [2]. In this paper transverse energy and charged particle flow were decomposed into nucleon and pion flow under a few simple assumptions. Both were studied as a function of pseudorapidity. Using these results and a simple parameterization of the proton and pion spectra in  $y$  and  $p_t$  from the AGS experiment E866 [22] and our own measurement [18] which together provide complete rapidity coverage, we evaluate  $\langle p_x \rangle$  as a function of rapidity. More specifically, we parameterize the spectra by expressions of the form:

$$\frac{d^2 N}{m_t dm_t dy} \propto \exp\left(-\frac{(y - y_0)^2}{2 \cdot \sigma_y^2}\right) \cdot m_t \exp\left(-\frac{m_t - m}{T_b(y)}\right), \quad (12)$$

and

$$T_b(y) = T_0 \exp\left(-\frac{(y - y_0)^2}{2 \cdot \sigma_T^2}\right) \quad (13)$$

with values of  $\sigma_y = 0.89$  (0.88),  $T_0 = 0.26$  (0.15) GeV, and  $\sigma_T = 1.06$  (1.70) for protons (charged pions). Using these parameterizations we calculate the mean rapidity  $y(\eta)$  (weighted with  $E_T$ ) and the width of the rapidity interval associated with a bin in pseudorapidity. Then, under the assumption that  $v_1^{E_T}$  and  $v_1^{p_t}$  are similar, one obtains  $\langle p_x \rangle$  as a function of rapidity:

$$\langle p_x(y) \rangle \approx \langle p_t(y) \rangle \cdot v_1^{E_T}(y). \quad (14)$$

The resulting mean transverse momenta are presented as stars in Fig. 11, together with our spectrometer results, for protons and pions; the errors shown are a propagation of the statistical errors in the measured flow of  $E_T$  and  $N_c$ . The horizontal error-bars shown with the stars represent the widths of the rapidity region actually contributing to the pseudorapidity bins for which  $v_1$  was measured.

Overall, the agreement between the results of the current analysis of spectrometer data at forward (and backward) rapidities and the results derived from the measurements of  $E_T$  and  $N_c$  flow is good. For the latter method we had estimated the systematic error for proton flow to be about 10% [2]; this can also be judged from the symmetry of the data shown in Fig. 11 with respect to midrapidity (note that all stars correspond to measured points). The dotted line has been added to aid inspection of the data for the necessary antisymmetry. The first and the next to last proton point have equal distance from mid-rapidity and should be identical. They differ by 10 MeV/c (out of 80 MeV/c). For the spectrometer results the systematic errors are largest at the lowest rapidities shown (see Fig. 9 and discussion) where they are estimated to be 20 MeV/c.

Within these errors the points obtained from the two methods merge smoothly and taken together they provide a measurement of  $\langle p_x \rangle$  for protons and charged pions as a function of rapidity over practically the entire relevant rapidity range. One can see a proton flow signal rising away from midrapidity to maximal values of about 130 MeV/c close to beam and target rapidities. The pion signal is in comparison very small, about 1/20 or the proton signal, but nevertheless significant. It is directed opposite to the nucleon flow signal.

### Comparison with RQMD predictions

In Fig. 11 we compare our results for  $\langle p_x \rangle$  with the predictions of the RQMD event generator [17,10], versions 1.08 and 2.3. Version 1.08, run in cascade mode, has been used for comparison to our earlier results for Au + Au collisions on pseudorapidity distributions [23], proton and pion rapidity [18] and transverse mass [15] distributions as well as results for Si+A and p+A collisions. For the Au + Au system it was found that overall many features

of the data are predicted correctly with one striking deviation: generally proton spectra are significantly too steep in the model; at midrapidity the inverse slope constant is only 2/3 of the experimental value. Predictions from this version of the model have also been compared to our experimental results for flow in  $E_T$  and  $N_c$  [1,2] and generally the model exhibited too little flow as compared to the data. Comparing to the proton data in Fig. 11, we find that the model also underpredicts the proton flow by nearly a factor of two. For pions, the sign change of the flow relative to protons is properly predicted but in magnitude the model overpredicts this opposite pion flow by a factor of 2 to 3.

Meanwhile, a new version of RQMD (version 2.3) has been developed [10]. It has been known for some time [24] that taking into account mean field effects by simulating in the model a Skyrme-type nucleon-nucleon potential increases the slopes of proton spectra and at the same time increases the proton flow signal while reducing the opposite pion flow signal in magnitude. We have used the most recent version of the model in the so-called “mean field” mode to compare to the present data as well. Indeed, in this version of the code the proton flow signal is larger by about 50% for the proton  $\langle p_x \rangle$  at the peak and the data are described rather well (see Fig. 11). Simultaneously, the opposite pion flow is reduced, again to a level consistent with the experimental data. It should be noted that at the same time the slope difference in the proton spectra is reduced (at midrapidity the slope constant of the model is now 3/4 of what is observed in the data) but a deviation persists at all rapidities.

Fig. 12 shows that the agreement of the RQMD predictions (version 2.3, mean field) with the experimental results for  $\langle p_x \rangle$  of protons as displayed in Fig. 11 may indeed be accidental. The functional dependence of the proton flow signal, expressed now in terms of the first Fourier coefficient  $v_1$  as a function of  $p_t$ , is very different from what is seen in the data. In the model, the flow signal rises at first with increasing  $p_t$  and then becomes rather flat. In fact, in the rapidity bin around  $y = 2.9$  the model overpredicts  $v_1$  but at the same time underpredicts the overall slope of the proton spectrum by 25 % giving overall agreement in  $\langle p_x \rangle$ . An interesting question arises whether the rapidly rising and saturating  $p_t$  dependence as exhibited by the RQMD predictions (which is in fact a general trend observed for all rapidity bins) is due to the rescattering-type mechanism which produces flow in a cascade code in contrast to a hydrodynamic flow mechanism (reflected *e.g.* by the

$p_t$  dependence of Equations (10,11)).

The elliptic flow signal seen in the anisotropy of  $E_T$  and  $N_c$  was found to be in good agreement with the RQMD (version 1.08) prediction in our previous publication [2]. As discussed above, the sign of this elliptic flow signal changes from negative (preferential emission perpendicular to the reaction plane) at lower beam energies (1-2 GeV/nucleon range at the Bevalac and SIS) to a positive signal (preferential in-plane emission) at the present energy. It was recently noted by Sorge [9] that the  $v_2$  anisotropies are sensitive to the pressure at the maximum compression. Positive values of  $v_2$  were in fact predicted in a hydrodynamic model by Ollitrault for very high energies [11]. The observed change in sign between Bevalac/SIS and AGS energies therefore implies that at AGS energies already the final in-plane flow overwhelms the initial shadowing effect. It would be interesting to deduce, from this information, the pressure achieved at maximum baryon density in Au + Au collisions at the AGS.

## VI. SUMMARY AND CONCLUSION

The measured flow signals of identified particles show that, in semi-central collisions, protons (nucleons) exhibit strong directed flow. Pions of low  $p_t$  exhibit flow in the opposite direction; at higher  $p_t$  pions start to flow in the same direction as protons. The results on  $\langle p_x \rangle$  values for proton and pion are complementary in acceptance and match well with nucleon and pion flow values derived from the same experiment by measurement of  $E_T$  and  $N_c$  flow [2]. Taken together, these results represent a directed flow measurement of protons and pions over nearly the entire rapidity region in Au+Au collisions at 11A GeV/c. The flow is found to be maximal around beam and target rapidities with values of  $\langle p_x \rangle$  for protons of about 130 MeV/c and 5% of that for charged pions.

The observed positive values of the second harmonic amplitudes of the proton azimuthal distributions correspond to preferential particle emission in the reaction plane. This observation agrees with our previous measurements of  $E_T$  and  $N_c$  elliptic flow [2].

The nearly linear dependence of the proton flow signal  $v_1$  on  $p_t$  can be interpreted in the framework of a transversely moving thermal source. The corresponding source velocity  $\beta_x$  appears to reach values of 0.1 in the beam rapidity region and for semi-central collisions.

The more complicated  $p_t$  dependence of the pion flow signals indicates that the effect there is probably a superposition of several effects such as absorption, Coulomb interaction and overall motion of the source (as for protons).

## ACKNOWLEDGMENTS

We thank the AGS staff, W. McGahern and Dr. H. Brown for excellent support and acknowledge the help of R. Hutter in all technical matters. Financial support from the US DoE, the NSF, the Canadian NSERC, and CNPq Brazil is gratefully acknowledged. One of us (JPW) thanks the A. v. Humboldt Foundation for support, while another (WCC) acknowledges the financial support from the Gottlieb-Daimler and Karl-Benz-Stiftung during his stay in Heidelberg, Germany, where part of this work was done.

## APPENDIX

### Flattening of the Reaction Plane Distribution

We apply the following procedure to correct for the non-flatness of the reaction plane distribution. Any flattening of the distribution means a correction to the reaction plane angle. We explicitly introduce this correction defining a new angle as:

$$\Psi'_1 = \Psi_1 + \Delta\Psi_1. \quad (15)$$

where  $\Delta\Psi_1$  is written in the form:

$$\Delta\Psi_1 = \sum_n (A_n \cos(n\Psi_1) + B_n \sin(n\Psi_1)) \quad (16)$$

Requiring the vanishing of the  $n$ -th Fourier moment of the new distribution, the coefficients  $A_n$  and  $B_n$  can be evaluated by the original distribution.

$$B_n = \frac{2}{n} \langle \cos(n\Psi_1) \rangle, \quad (17)$$

$$A_n = -\frac{2}{n} \langle \sin(n\Psi_1) \rangle, \quad (18)$$

where the brackets refer to an average over events. This gives:

$$\Psi'_1 = \Psi_1 + \sum_n \frac{2}{n} ( -\langle \sin(n\Psi_1) \rangle \cos(n\Psi_1) + \langle \cos(n\Psi_1) \rangle \sin(n\Psi_1) ) \quad (19)$$

In practice, we flatten the reaction plane distribution up to the fourth harmonic ( $n=4$ ). Note that, due to the small values of  $A_n$  and  $B_n$  (typically of the order of a few percent), such a flattening of the distribution does not have any effect on the reaction plane resolution. It can also be shown that the same flattening procedure removes possible trigger biases (due to imperfect calibration, dead channels or any other asymmetry) at least up to the second order.

## FIGURE CAPTIONS

1. The E877 apparatus.
2. Proton  $m_t$  distributions in the rapidity interval  $2.8 < y < 2.9$  for different centralities (indicated by an  $E_T$  range in GeV) together with a fit using the function given in Equation (4). The inverse slope values and their statistical errors are shown in GeV. The open (filled) squares correspond to  $-\pi/4 < \phi < \pi/4$  ( $3\pi/4 < \phi < 5\pi/4$ ).
3. The dependence of the inverse (Boltzmann) slope  $T_B$  of the proton distributions as a function of azimuthal angle. The open points are reflections of the filled points about  $\phi = 0$ .
4. The transverse momentum dependence of the first moment ( $v_1$ ) of the proton azimuthal distributions for different particle rapidities and centralities of the collision. The solid and dashed curves are fits using functions given in Eqs. (11) and (6), respectively. For a description see Sections IV and V.
5. Same as Fig. 4 for  $\pi^+$ .
6. Same as Fig. 4 for  $\pi^-$ . The open and filled symbols correspond to data from the 1993 and 1994 runs.
7. Fourier coefficients  $v_1$  for pions in the low  $p_t$  region for the rapidity interval  $3.2 < y < 3.6$  and two different centralities. Solid symbols represent data for positive pions. Open symbols are for negative pions (circles and squares correspond to results from the 1993 and 1994 runs, respectively).
8. The transverse momentum dependence of the second moment ( $v_2$ ) of the proton azimuthal distributions for different particle rapidities and centralities of the collision.
9. The mean projection  $\langle p_x \rangle$  of the proton transverse momentum onto the reaction plane as a function of rapidity for different centralities of the collision. Results for the second and fourth centrality bin are shifted to the left by 0.025 for clarity of the picture. Solid and open symbols correspond to fits of  $v_1(p_t)$  with functions given in Eqs. (11) and (6), respectively.

10. The transverse velocity  $\beta_x$  of a thermal (proton) source for different rapidities and centralities of the collision. For details see text.
11. Mean projection  $\langle p_x \rangle$  of the proton and pion transverse momentum onto the reaction plane as a function of rapidity for the centrality bin with  $E_T = 200-230$  GeV. Solid circles, squares, and triangles correspond to measurements in the spectrometer. Open circles, squares, and triangles are reflections of the filled symbols about midrapidity. The results derived from measurements of  $E_T$  and  $N_c$  flow [2] for nucleons and pions are shown by stars (see text). The dotted line is added to aid inspection of the solid stars for antisymmetry about mid-rapidity. Results from calculations using 2 versions of RQMD (1.08 in cascade mode, 2.3 in mean field mode) are depicted as histograms.
12. Comparison of measured values of  $v_1$  for protons in two rapidity bins and the centrality bin with  $E_T = 200-230$  GeV with those predicted by 2 versions of the event generator RQMD.

- 
- [1] J. Barrette *et al.*, E877 Collaboration, Phys. Rev. Lett. **73**, 2532 (1994).
- [2] J. Barrette *et al.*, E877 Collaboration, Phys. Rev. **C55**, 1420 (1997).
- [3] T. Wienold for the NA49 Collaboration, Nucl. Phys. **A610**, 76c (1996).
- [4] L. Bravina, L.P. Csernai, P. Lévai, and D. Strottman, Phys. Rev. **C50**, 2161 (1994); L. Bravina, Phys. Lett. **B344**, 49 (1995).
- [5] C.M. Hung and E.V. Shuryak, Phys. Rev. Lett. **75**, 4003 (1995).
- [6] B.A. Li, C.M. Ko, and G.Q. Li, Phys. Rev. **C54**, 844 (1996).
- [7] D.R. Rischke, Nucl. Phys. **A610**, 88c (1996).
- [8] B.A. Li and C.M. Ko, Phys. Rev. **C52**, 2037 (1995); Phys. Rev. **C53**, R22 (1996).
- [9] H. Sorge, Phys. Rev. Lett. **78**, 2309 (1997).
- [10] H. Sorge, in Proceedings of the Workshop "Heavy-Ion Physics at the AGS '96," eds. C.A. Pruneau, G. Welke, R. Bellwied, S.J. Bennett, J.F. Hall, and W.K. Wilson, Wayne State University, 1996.
- [11] J. Y. Ollitrault, Phys. Rev. **D46**, 229 (1992); Phys. Rev. **D48**, 1132 (1993).
- [12] S. Voloshin and Y. Zhang, Z. Phys. **C70**, 665 (1996);
- [13] D. Miśkowiec for the E877 Collaboration, Nucl. Phys. **A590**, 473c (1995); Nucl. Phys. **A610**, 227c (1996).
- [14] S.A. Voloshin and W.E. Cleland, Phys. Rev. **C53**, 896 (1996); Phys. Rev. **C54**, 3212 (1996).
- [15] J. Stachel, Nucl. Phys. **A610**, 509c (1996).
- [16] H. Gutbrod, K. H. Kampert, B. W. Kolb, A. M. Poskanzer, and H. G. Ritter, Phys. Lett. **B216**, 267 (1989); D. Brill *et al.*, Phys. Rev. Lett. **71**, 336 (1993); C. Pinkenburg and K.D. Hildenbrand, Acta Phys. Polonica **27**, 243 (1996); S. Wang *et al.*, Phys. Rev. Lett. **76**, 3911

(1996).

- [17] H. Sorge, A.v. Keitz, R. Mattiello, H. Stöcker, and W. Greiner, *Phys. Lett.* **B243**, 7 (1990).
- [18] R. Lacasse for the E877 Collaboration, *Nucl. Phys.* **A610** 153c (1996); J. Barrette *et al.*, E877 Collaboration, in preparation.
- [19] J. Barrette *et al.*, E877 Collaboration, *Phys. Rev. Lett.* **70**, 2996 (1993).
- [20] S.A. Voloshin, *Phys. Rev.* **C55**, 1630 (1997).
- [21] Review of Particle Physics, *Phys. Rev.* **D54**, 195 (1996).
- [22] Y. Akiba for the E802 Collaboration, *Nucl. Phys.* **A590**, 139c (1996).
- [23] J. Barrette *et al.*, E877 Collaboration, *Phys. Rev.* **C51**, 3309 (1995).
- [24] R. Mattiello, Doctoral Dissertation, Univ. Frankfurt, June 1995.

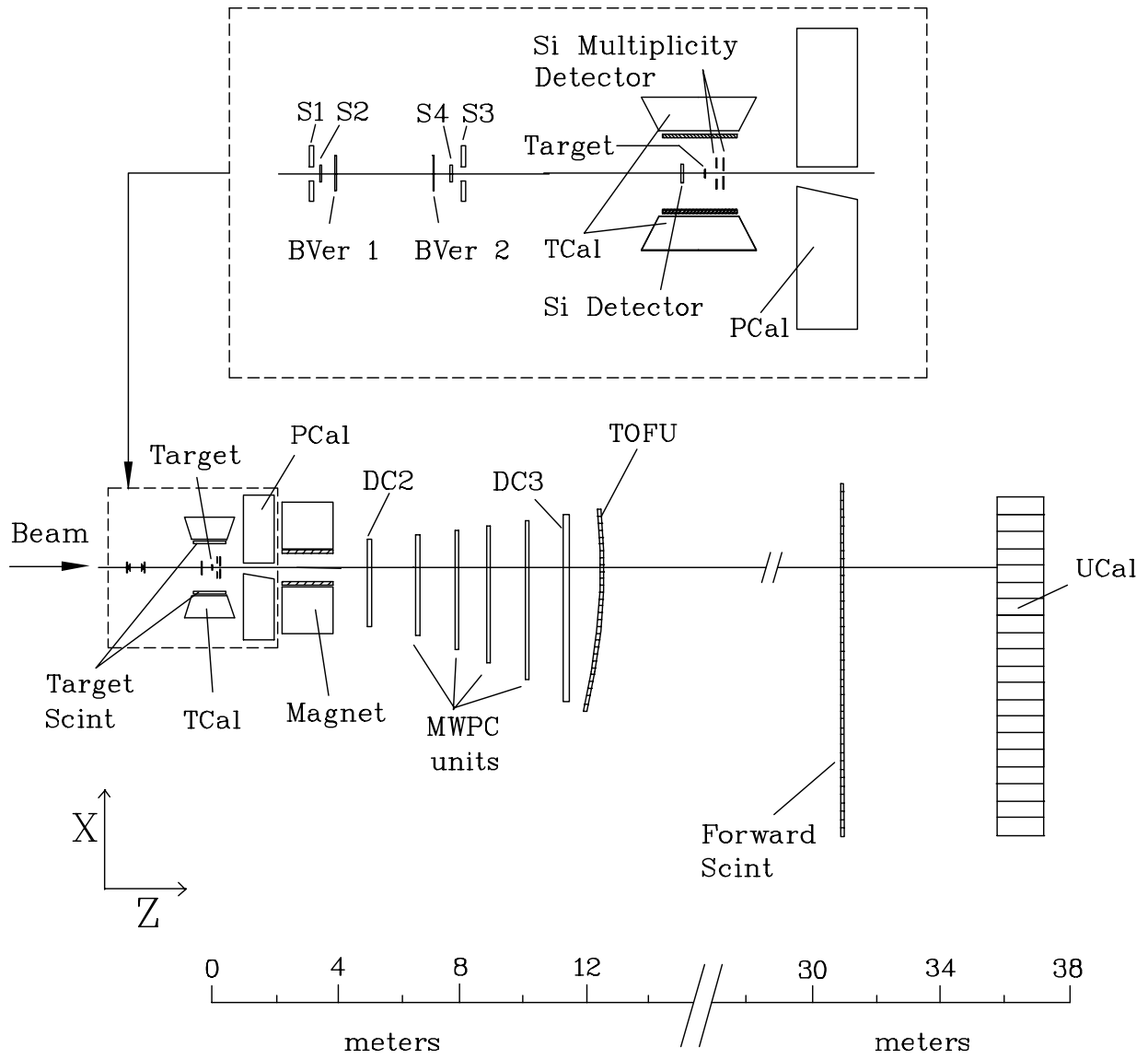


FIG. 1. The E877 apparatus.

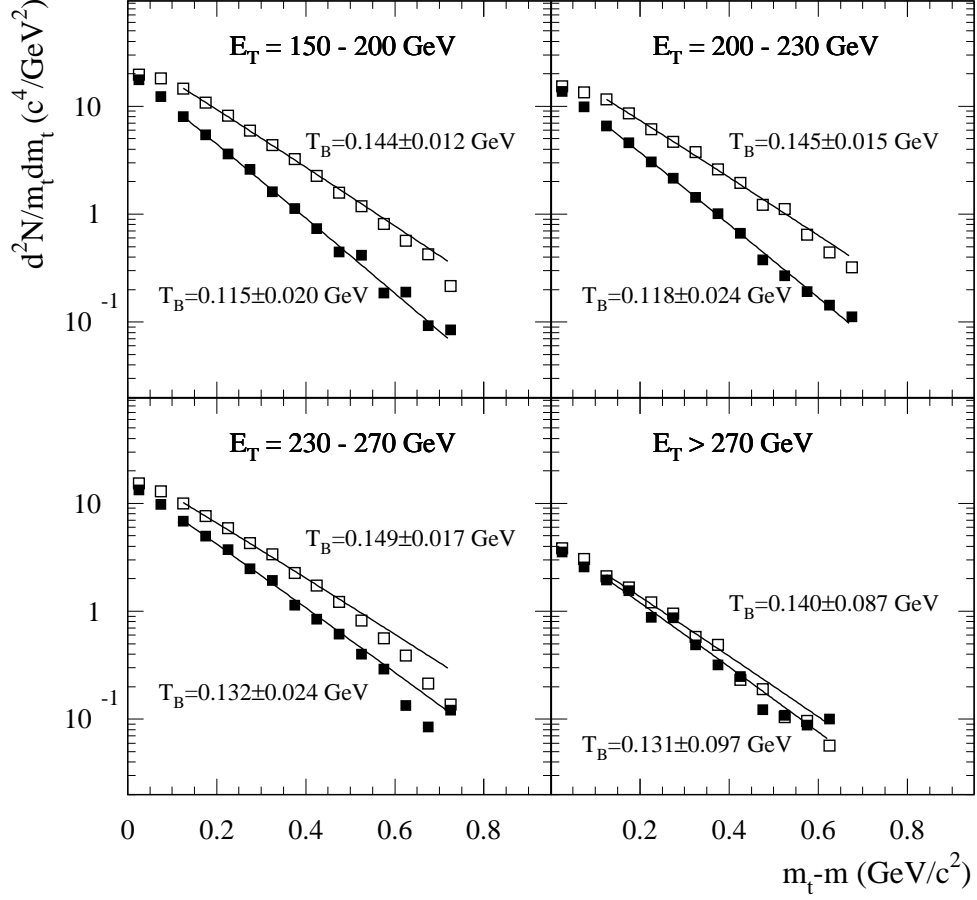


FIG. 2. Proton  $m_t$  distributions in the rapidity interval  $2.8 < y < 2.9$  for different centralities (indicated by an  $E_T$  range in GeV) together with a fit using the function given in Equation (4). The inverse slope values and their statistical errors are shown in GeV. The open (filled) squares correspond to  $-\pi/4 < \phi < \pi/4$  ( $3\pi/4 < \phi < 5\pi/4$ ).

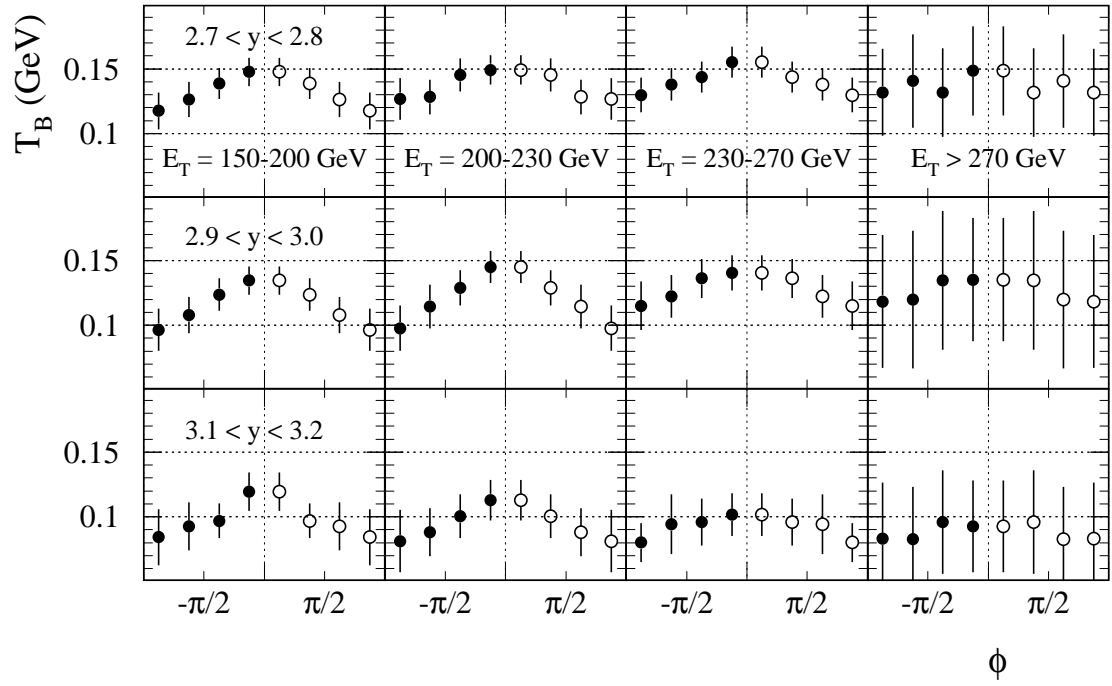


FIG. 3. The dependence of the inverse (Boltzmann) slope  $T_B$  of the proton distributions as a function of azimuthal angle. The open points are reflections of the filled points about  $\phi = 0$ .

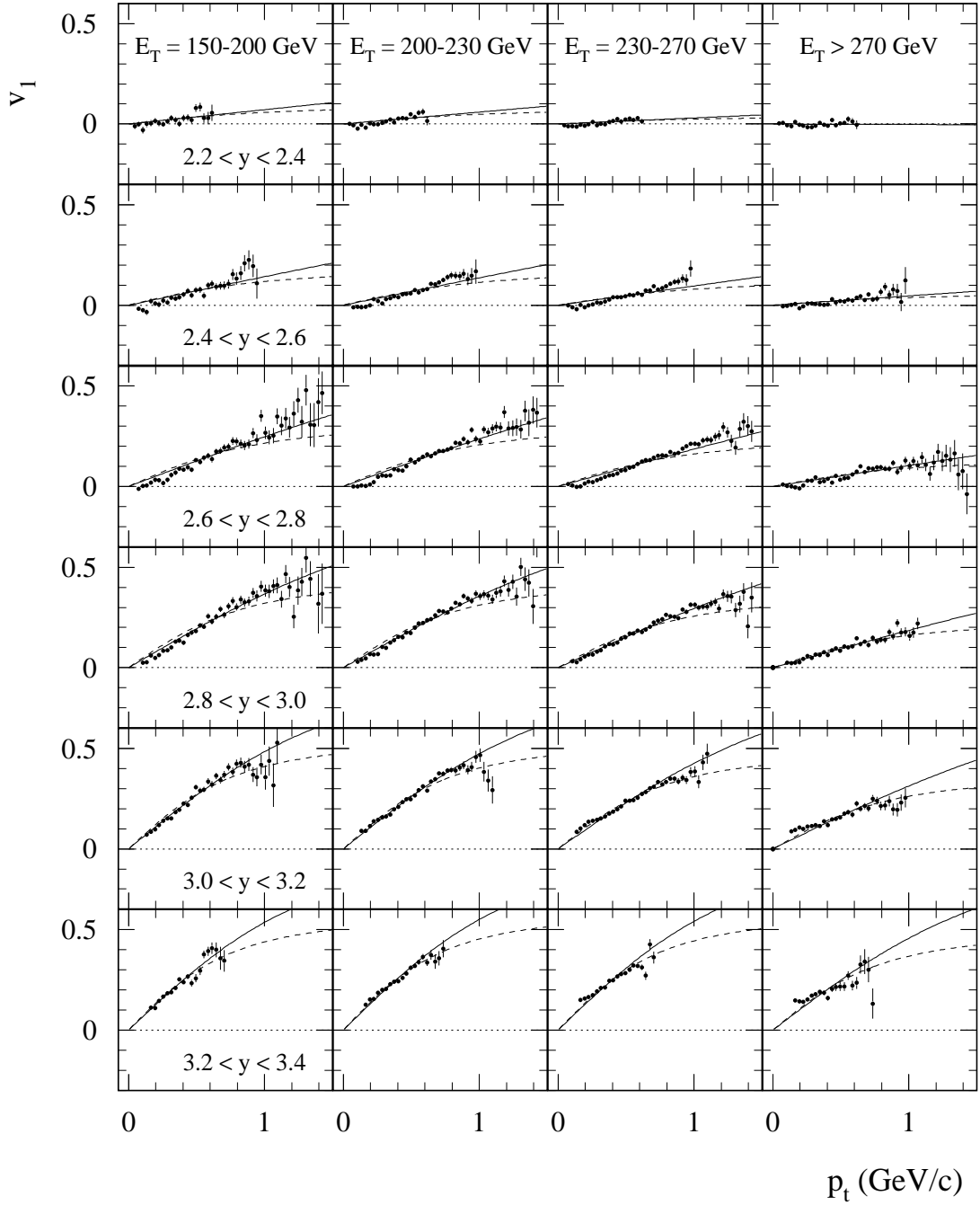


FIG. 4. The transverse momentum dependence of the first moment ( $v_1$ ) of the proton azimuthal distributions for different particle rapidities and centralities of the collision. The solid and dashed curves are fits using functions given in Eqs. (11) and (6), respectively. For a description see Sections IV and V.

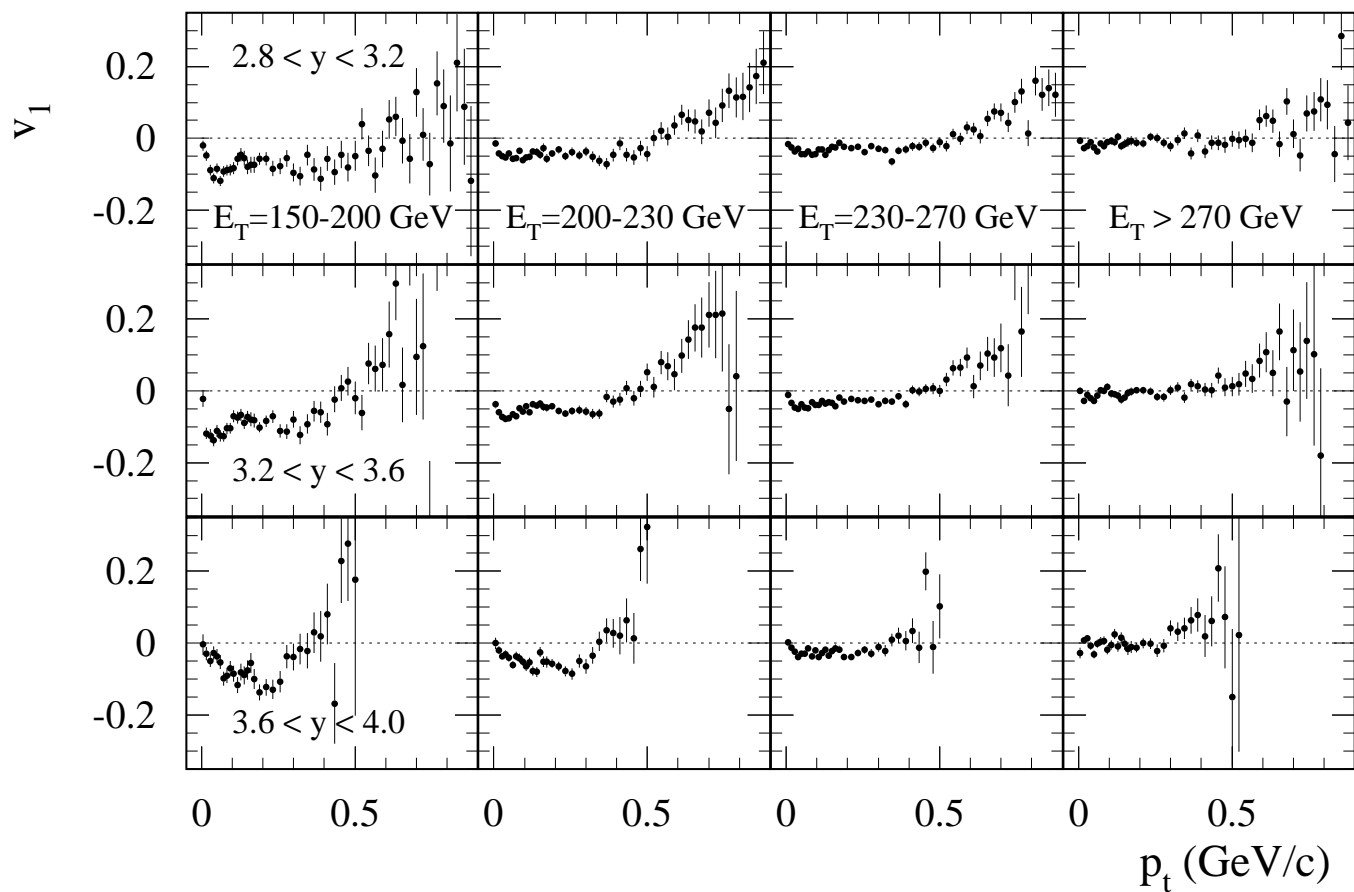


FIG. 5. Same as Fig. 4 for  $\pi^+$ .

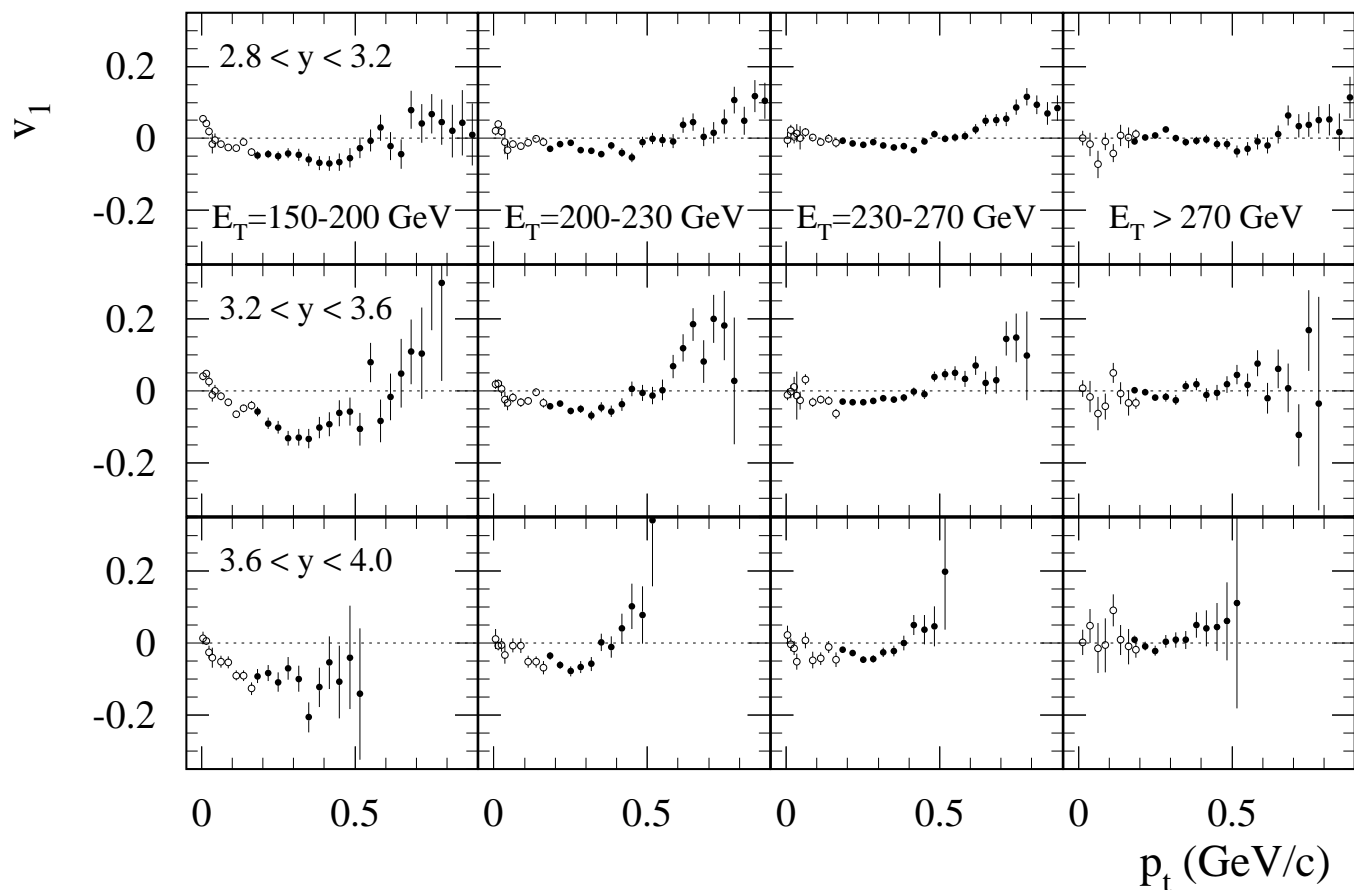


FIG. 6. Same as Fig. 4 for  $\pi^-$ . The open and filled symbols correspond to data from the 1993 and 1994 runs.

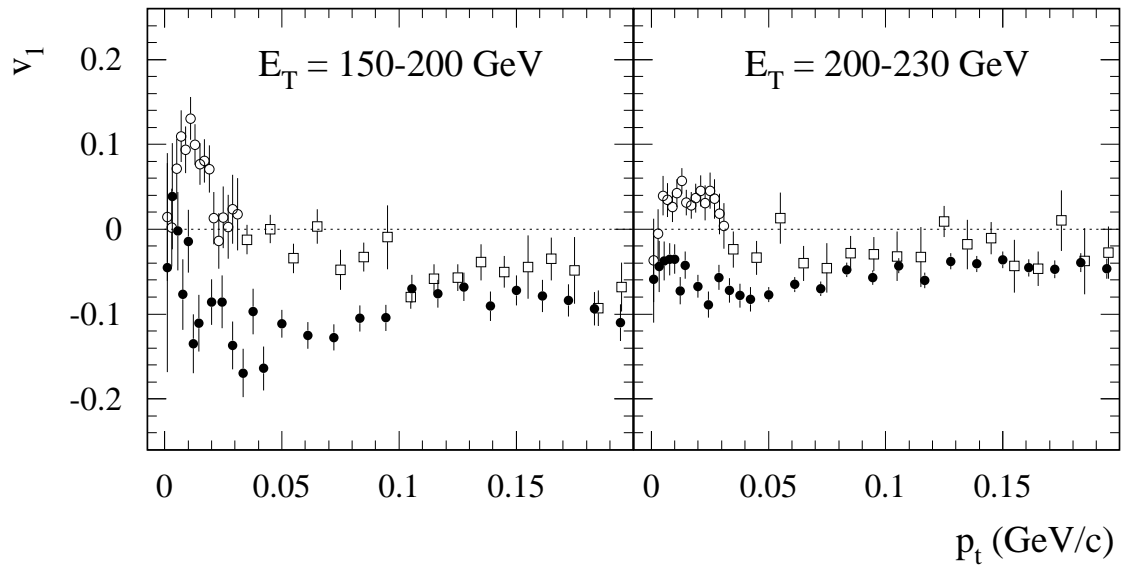


FIG. 7. Fourier coefficients  $v_1$  for pions in the low  $p_t$  region for the rapidity interval  $3.2 < y < 3.6$  and two different centralities. Solid symbols represent data for positive pions. Open symbols are for negative pions (circles and squares correspond to results from the 1993 and 1994 runs, respectively).

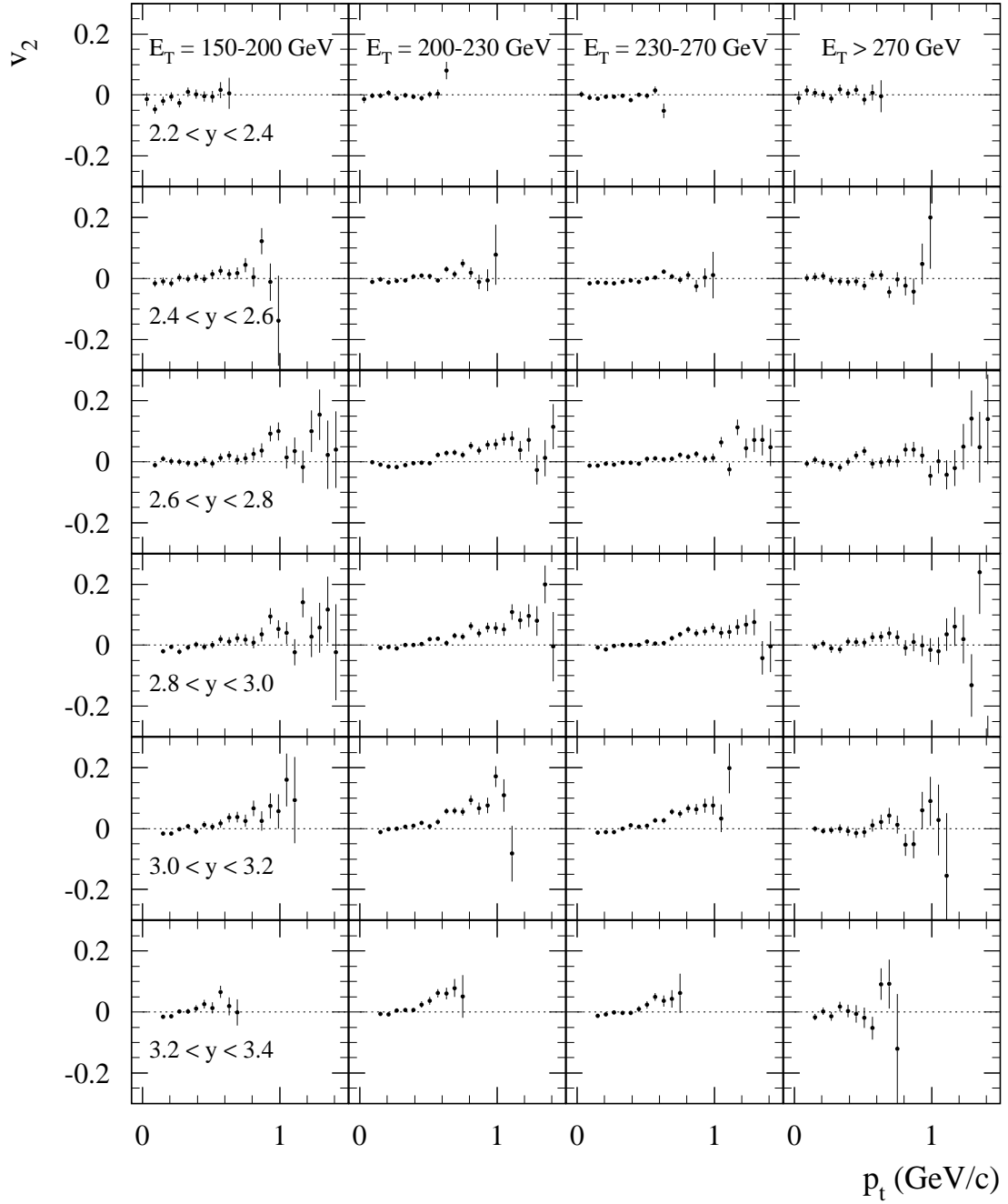


FIG. 8. The transverse momentum dependence of the second moment ( $v_2$ ) of the proton azimuthal distributions for different particle rapidities and centralities of the collision.

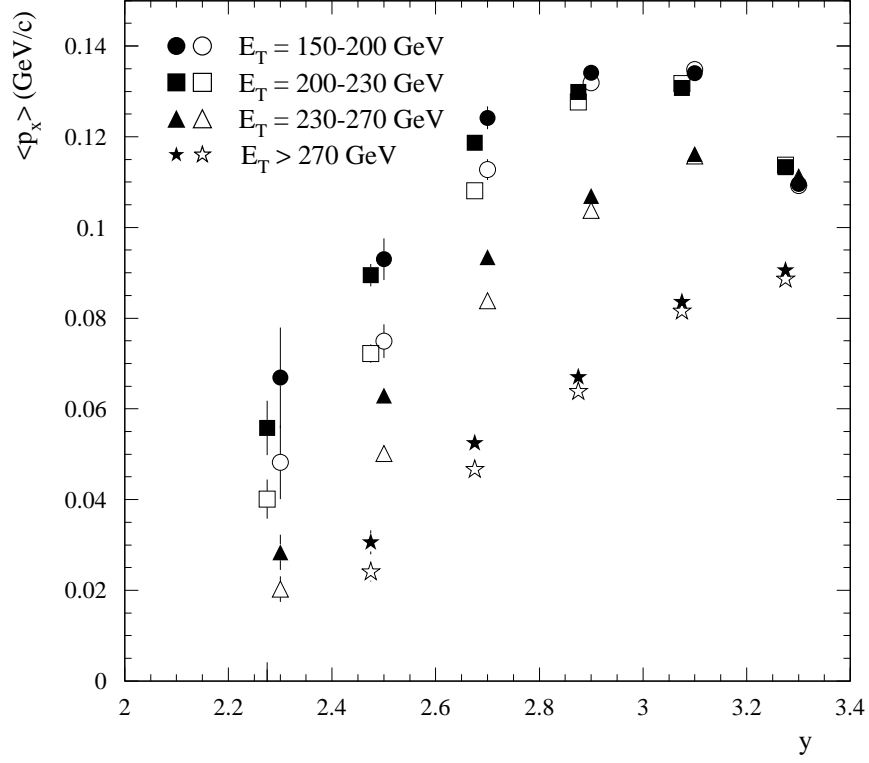


FIG. 9. The mean projection  $\langle p_x \rangle$  of the proton transverse momentum onto the reaction plane as a function of rapidity for different centralities of the collision. Results for the second and fourth centrality bin are shifted to the left by 0.025 for clarity of the picture. Solid and open symbols correspond to fits of  $v_1(p_t)$  with functions given in Eqs. (11) and (6), respectively.

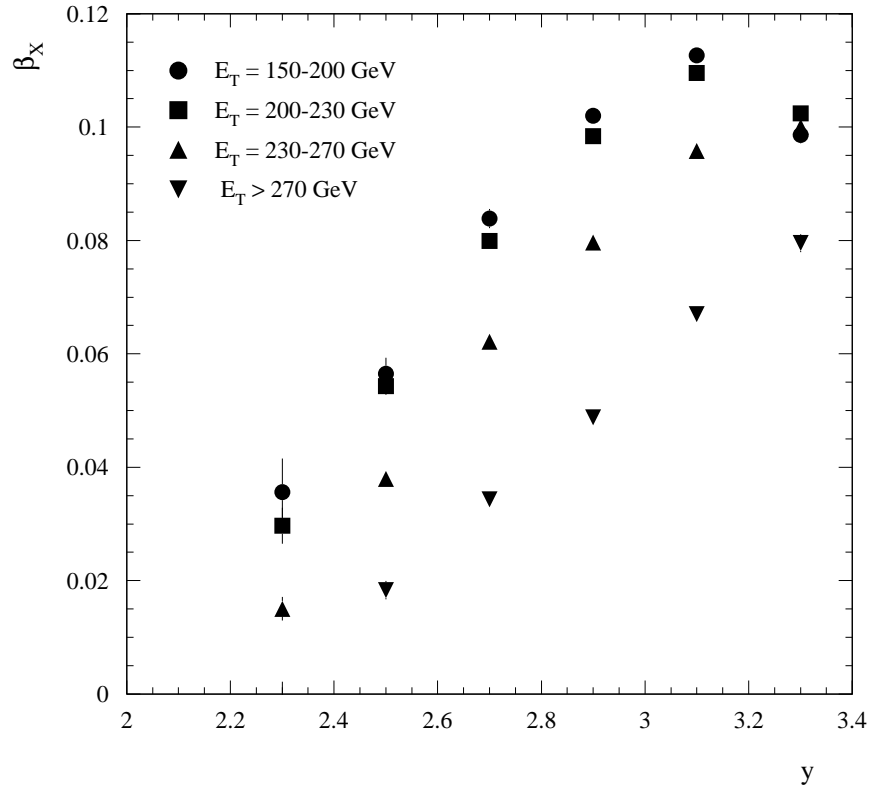


FIG. 10. The transverse velocity  $\beta_x$  of a thermal (proton) source for different rapidities and centralities of the collision. For details see text.

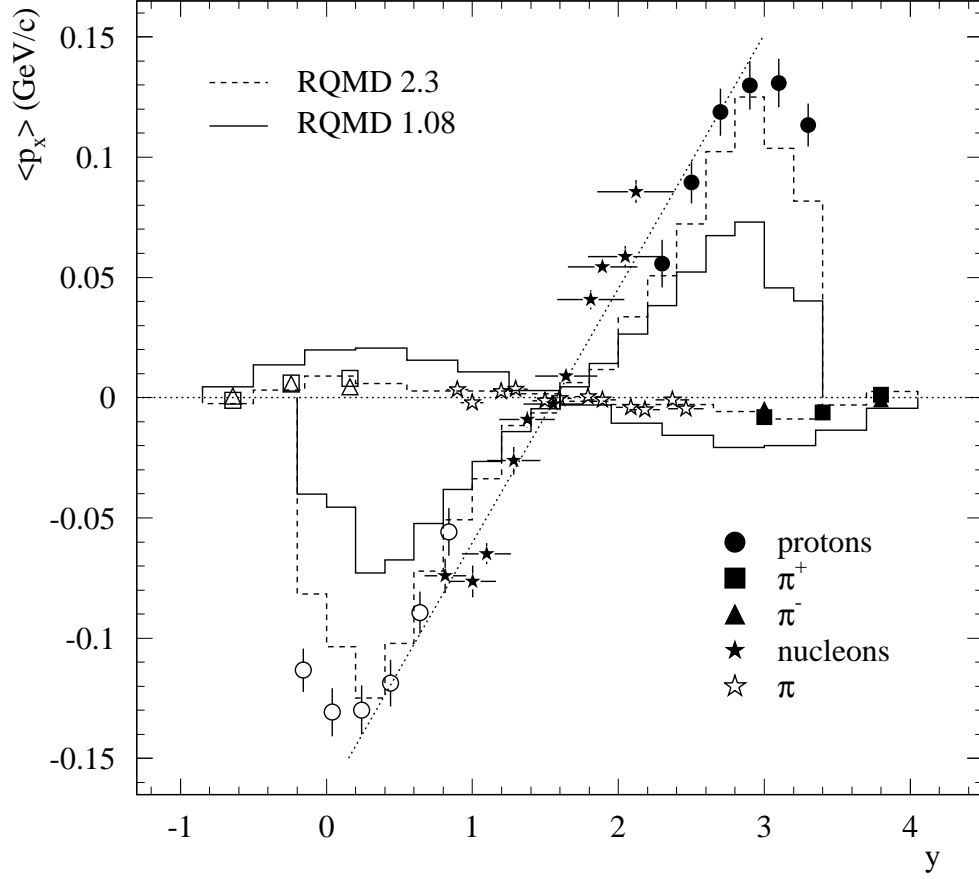


FIG. 11. Mean projection  $\langle p_x \rangle$  of the proton and pion transverse momentum onto the reaction plane as a function of rapidity for the centrality bin with  $E_T = 200-230$  GeV. Solid circles, squares, and triangles correspond to measurements in the spectrometer. Open circles, squares, and triangles are reflections of the filled symbols about midrapidity. The results derived from measurements of  $E_T$  and  $N_c$  flow [2] for nucleons and pions are shown by stars (see text). The dotted line is added to aid inspection of the solid stars for antisymmetry about mid-rapidity. Results from calculations using 2 versions of RQMD (1.08 in cascade mode, 2.3 in mean field mode) are depicted as histograms.

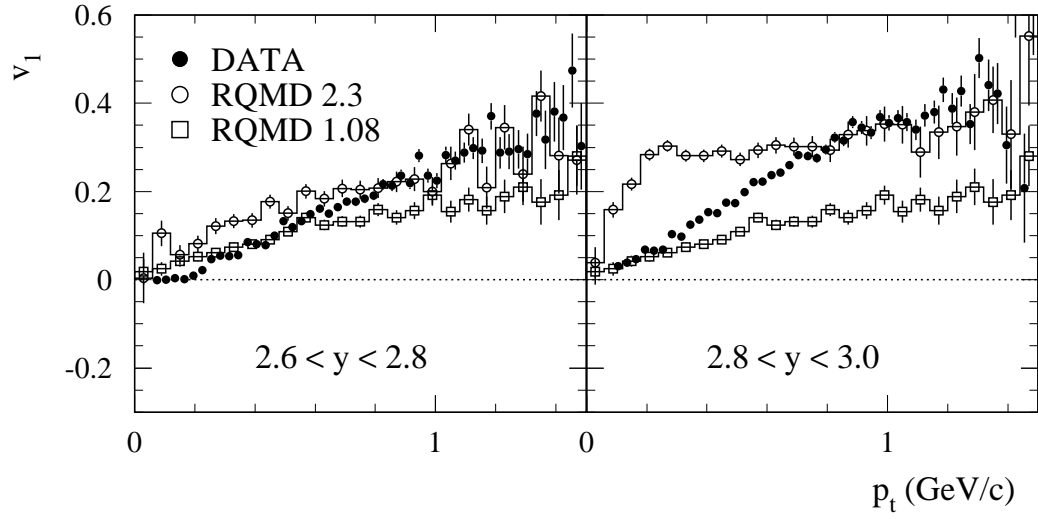


FIG. 12. Comparison of measured values of  $v_1$  for protons in two rapidity bins and the centrality bin with  $E_T = 200\text{-}230$  GeV with those predicted by 2 versions of the event generator RQMD.